Near-infrared imaging of artificial enamel caries lesions with a scanning fiber endoscope

Robert Chulsung Lee

A thesis

Submitted in partial fulfillment of the

Requirements for the degree of

Master of Science in Dentistry

University of Washington

2019

Committee:

Eric J. Seibel

Alireza Sadr

Burcu Bayirli

Program Authorized to Offer Degree:

Orthodontics

University of Washington

Abstract

Near-infrared imaging of artificial enamel caries lesions with a scanning fiber endoscope

Robert Chulsung Lee

Chair of Supervisory Committee

Eric. J. Seibel

Department of Mechanical Engineering

Department of Electrical and Computer Engineering

Department of Restorative Dentistry

Department of Orthodontics

Several studies have shown that near-infrared imaging has great potential for detection of dental caries lesions. A miniature scanning fiber endoscope (SFE) operating at near-infrared (NIR) wavelengths was developed and used in this study to test whether the device could be used to discriminate demineralized enamel from sound enamel. Varying depths of artificial enamel caries lesions were prepared on twenty bovine blocks with smooth enamel surfaces. Samples were imaged with a SFE operating in the reflectance mode at 1310-nm and 1460-nm in both wet and dry conditions. The measurements acquired by the SFE operating at 1460-nm show significant difference between the sound and the demineralized enamel. There was a moderate

positive correlation between the SFE measurements and micro-CT measurements, and the NIR SFE was able to detect the presence of demineralization with high sensitivity (0.96) and specificity (0.85). This study demonstrates that the NIR SFE can be used to detect early demineralization from sound enamel. In addition, the NIR SFE can differentiate varying severity of demineralization. With its very small form factor and maneuverability, the NIR SFE should allow clinicians to easily image teeth from multiple viewing angles in real-time.

Dedication

This thesis is dedicated to my wife, Jinny, who offered unconditional love, support and encouragement.

Acknowledgements

This work was supported by an exploratory grant from the National Institute of Health NIDCR R21-DE025356, the National Science Foundation award 1631146 and the UW Orthodontics Alumni Association.

Foremost, I would like to express my sincere gratitude to my thesis advisor, Dr. Eric Seibel, for the continuous support, patience, motivation, enthusiasm, knowledge and guidance during the last three years.

Besides my thesis advisor, I would like to thank members of my thesis committee: Drs. Alireza Sadr and Burcu Bayirli. I am very grateful for their brilliant comments.

My sincere thanks go to the members of Human Photonics Lab, Biomimetics Biomaterials Biophotonics Biomechanics & Technology Lab and Fried Lab. I would like to also acknowledge contributions from Dr. Daniel Fried, Yaxuan Zhou, Sara Finkleman, Cathy Olivio, Mathew Carson, Minh Tran, and William Tressel. Much of my experimental work could not have been completed without their help.

I am grateful to the University of Washington Department of Orthodontics for offering me an excellent education, a research opportunity and a valuable guidance throughout my clinical and research training. I am also thankful to Taryn Sanders-Sheats and Bette Horishige for their administrative support through the program.

Table of Contents

1 Introduction

Since the introduction of water fluoridation in the 20th century, the prevalence and severity of dental caries has been constantly decreasing in the United States [1,2]. In addition to water fluoridation, improved oral hygiene and access to dental care, as well as the increased availability of fluoride dentifrices and professional fluoride applications have all contributed to this shift in caries trends [3,4]. However, dental caries remains a significant problem in the United States [1,5,6]. The majority of newly discovered caries lesions are located in pits and fissures of posterior teeth and on interproximal surfaces between adjacent teeth where they are difficult to detect [7-9]. If caries lesions are detected early, they can be treated via non-surgical interventions and loss of tooth structure is avoided [10,11].

Early signs of enamel caries lesions are initially seen as "white spot lesions" (WSLs). White spot lesions are increasingly common among children, especially those who go through orthodontic treatment [12]. WSLs have subsurface demineralization with increased porosity, which often cause changes in the optical properties of enamel and can be aesthetically displeasing [12]. WSLs typically form around high plaque stagnation areas such as gingival margins, pits, and interproximal surfaces of teeth, and intraoral appliances such as orthodontic brackets and bands. If caries lesions are detected early, non-surgical treatment options to reverse the caries process such as topical fluoride and calcium phosphate-based remineralization agents can be implemented before the lesion has progressed [13]. Therefore, the timely diagnosis of caries and detection of early demineralization is critical.

Current methods for caries lesion detection and assessment are composed of a combination of visual and tactile exams, which are prone to subjective bias and interference from surface staining. In addition, visual and tactile exams are limited to exposed surfaces, and there is the

potential for permanently damaging the intact lesion surface layer from sharp dental instruments [14,15]. Intraoral radiography is most commonly used as an adjunct to visual and tactile examinations for the evaluation of proximal and occlusal caries lesions. Although intraoral radiography is highly specific in detecting advanced caries lesions, its sensitivity is low as intraoral radiography is not capable of showing very early stages of demineralization [16,17]. Moreover, intraoral radiography can be technique-sensitive: overlapping crown structures and radiopaque materials, such as restorative materials and orthodontic appliances, can interfere with imaging, making caries detection difficult. In addition, the risk of exposure to ionizing radiation cannot be underestimated. Therefore, there has been an emphasis on the need for new caries detection techniques that allow for real-time imaging to monitor the progression of early caries lesions [18,19].

Optical diagnostic methods exploit changes in the fluorescence or light scattering of the caries lesion and therefore have great potential for the detection and assessment of caries lesions [20,21]. Near-infrared (NIR) spectrum is the ideal range for high contrast imaging of dental caries due to increased light scattering to caries affected dental tissue [22]. Previous studies have shown transparency of sound enamel in the NIR wavelength, where the attenuation coefficient is 20 to 30 times lower than that in the visible region [23,24]. Recent studies on NIR reflectance imaging with wavelengths coincident with high water absorption, at 1460-nm and beyond 1500-nm, demonstrated high lesion contrast for artificial and natural enamel caries lesions, while also eliminating the influence from stains, which are common in visible-light imaging [25,26].

Scanning fiber endoscope (SFE) uses fiber-scanning-based imaging technology to produce high-quality multi-spectral video. Several studies have demonstrated that SFE can be used intraorally to nondestructively image tooth demineralization. Zhang et al. demonstrated that SFE

can be used for reflectance and fluorescence imaging of teeth at 405-nm and 532-nm wavelengths [27]. In addition, the SFE using the visible light wavelength was successfully evaluated for its clinical feasibility in a follow-up study [28]. The NIR wavelength has great potential to be employed as a light source for the SFE for detecting caries lesions in a clinical setting [19,29]. We recently developed a SFE operating at 1460 and 1310-nm wavelengths in reflectance mode for high contrast deep artificial lesions [30]. The prototype NIR laser-based SFE device should be able to generate high quality images of shallow artificial lesions with the same magnitude smaller form factor (1.6 mm SFE probe vs. 25 mm diameter NIR camera) at a significantly lower cost. Importantly, the NIR SFE small diameter is the size of a round toothpick and is small enough to fit around interproximal surfaces and intraoral appliances, such as orthodontic brackets, as shown in Figure 1. With the small form factor and maneuverability, the NIR SFE should allow clinicians to easily image teeth from multiple viewing angles in real-time.

The purpose of the study is to test the hypothesis that artificial enamel caries lesions can be discriminated from sound enamel using the NIR SFE reflectance imaging. Simulated caries lesions created using artificial demineralization will be used to assess the performance of the new NIR SFE device. The current study presents preliminary data on the ability of the NIR SFE device to accurately detect lesions at varying depths. If proven successful, the development of this new NIR SFE could have implications for detection and management strategies for early caries lesions. The null hypothesis is that NIR SFE cannot distinguish artificial lesions from sound enamel.

2 Materials and Methods

All bovine teeth used in this study was obtained *postmortem* from discards of animals raised for commercial slaughter. This study did not require the approval of an animal research ethics committee.

2.1 Sample Preparation

Based on effect size of 0.75 derived from a previous study, alpha of 0.05 and power of 0.95, minimum of 40 samples were needed for this study [31]. Twenty bovine mandibular central incisors were acquired from a slaughterhouse; each tooth was originated from a different cattle. Twenty bovine enamel blocks were prepared 8–12-mm in length with a width of 3-mm and a thickness of 3-mm. The facial surfaces of the bovine enamel blocks were ground to a 9-µm finish. Each bovine enamel sample was partitioned into five windows (1 sound and 4 lesion windows) by creating thin trough lines approximately 1.5-mm apart across using a 392 bur. Total sample size used in this study was 100. Each sample was mounted on a 1-cm × 1-cm × 1-cm black polyoxymethylene block.

The order of the five windows was randomized using a random number generator. A thin layer of acid-resistant varnish in the form of nail polish, Revlon (New York, NY) was applied to the sound window to prevent exposure to the demineralization solution. Samples with four exposed windows were immersed in a demineralization solution maintained at 37°C at pH 4.9 composed of a 40-mL aliquot of 2.0-mmol/L calcium, 2.0-mmol/L phosphate and 0.075-mol/L acetate. Acid-resistant varnish was applied to each window after 8, 16, 24 and 32-hours of demineralization to protect it from further demineralization. After the 32-hours of demineralization, the samples were removed from the demineralization solution, and the acid

resistant varnish was removed by immersion in acetone in an ultrasonic bath for 15-minutes. Each sample was stored in 0.1% thymol solution to prevent fungal and bacterial growth.

2.2 Near-infrared Scanning Fiber Endoscope (NIR SFE)

As shown in Figure 2, a single-mode fiber cantilever (SM1250G80, Thorlabs Inc., Newton, NJ) and a custom piezo tube actuator are mounted by collar in the center of the probe housing [30]. In each imaging frame, four piezo tube electrodes apply sinusoidal signals with phase difference and increasing amplitudes on the actuator. Then the actuator drives the central fiber cantilever to scan in an increasing spiral pattern. NIR SFE uses 1310-nm (LPSC-1310-FC, Thorlabs Inc., Newton, NJ) and 1460-nm (QFBGLD-1460-150, Thorlabs Inc., Newton, NJ) lasers as the light source. The scanning laser beam is focused onto the target by a lens assembly encapsulated in the probe tip. Backscattered light is then collected in a non-confocal manner by ten multi-mode fibers (FPL1009S, Thorlabs Inc., Newton, NJ) mounted around the scanner housing. InGaAs-based near-infrared photodiode (FGA21, Thorlabs Inc., Newton, NJ) is used to measure the intensity of collected backscattering light. As the central scanning fiber scans 250 spirals with increasing deflection amplitude and then is driven back to center by braking signal, a frame is generated by mapping the intensity at each position to its corresponding pixel. The frame rate is currently at 7-Hz and can be increased to 30-Hz for video-rate imaging. The probe has a diameter of 1.6-mm and a rigid length of 9-mm imposed by the piezo tube actuator and lens assembly. With the design of the fiber scanner, the SFE probe is over 800 times smaller in volume than the smallest commercial InGaAs camera (MQ022HG-IM-SM5X5-NIR, XIMEA, Münster, Germany). The probe also provides sufficient image quality with a 60-degree

expandable field of view. Spatial resolution is highest (35-μm) at a working distance of 2-mm and decreases with enlarged image size and greater separation distance.

The probe was mounted at an angle of approximately 30-degrees in order to avoid specular reflection from the sample surface. The probe to sample distance was approximately 5-mm. Four sets of images were taken using the NIR SFE: wet at 1310-nm, dry at 1310-nm, wet a 1460-nm and dry at 1460-nm. Wet samples were removed from 0.1% thymol solution and placed in a sample mount. A folded sheet of Kimwipe™ (Kimberly-Clark, Irving, TX) was placed near the edge of each sample to allow for absorption of the excess water on the surface. The 5 windows on each sample were imaged in separate frames using both 1310-nm and 1460-nm lasers from the left to right window. After imaging the wet samples, the samples were dried with pressurized air for 5 seconds and the imaging sequence was repeated.

2.3 NIR SFE Image Analysis

Images obtained from the NIR SFE were automatically analyzed using a dedicated program constructed with Labview™ (National Instrument, Austin, TX) software. A region of interest (ROI), 20 × 20 pixel (approximately 700μm × 700μm), was specified for the sound region of each sample in order to discriminate between demineralized and sound enamel. To minimize variation in angulation of incident light and specular reflection, the same ROI was selected for each window and the mean was recorded. The following measurements were recorded: raw intensity measurement at dry, raw intensity measurement at wet, raw intensity measurement difference between dry- and wet-conditions, and lesion contrast measurement. The lesion contrast was calculated using $(I_L - I_S)/I_L$ [32].

Once the most optimal method for NIR SFE analysis was identified, the measurements of the lesion windows from that specific method were subtracted by the measurement of their corresponding sound windows for the linear regression analysis versus μCT measurements. This relative raw intensity measurement calculation was done to normalize the NIR SFE optical measurement values based on the sound measurements as reference measurements.

The performance of the NIR SFE prototype was also evaluated for the most optimal method. Each window of the sample was ranked in an increasing order of measurements and the lowest ranking window was considered as a sound window. Sensitivity and specificity analysis at each time point of demineralization was performed.

2.4 Micro Computed Tomography (μCT), Lesion Depth and Relative Integrated Mineral Loss (ΔZ)

The μCT (X5000, North Star Imaging, Rogers, MN) images were acquired by a trained engineer at the Computed Tomography Facility at the University of Washington. A previous study has shown that μCT can be used as a non-destructive alternative to transverse microradiography with comparable parameters for the study of enamel lesions [33]. The x-ray source was set at 58-kV, 231-μA and 13.4-μm focal spot size. The detector panel has pixel pitch of 200-μm × 200-μm. The distance between the x-ray source and the sample was 28.9-mm, the distance between x-ray source and the detector was 454.57-mm, and the zoom factor was 15.7. Each sample was mounted on a custom 3D-printed holder to ensure proper and repeatable positioning for imaging. 720 projections were acquired on each sample in approximately 36-minutes.

Image reconstruction was initially performed using the default software of the system (efX, North Star Imaging, Rogers, MN). efX is proprietary software that performs automatic calibration for reconstruction process optimization. A physical geometry tool is scanned to avoid common errors with manipulator type of calibration (i.e., geometry issues, system accuracy derivation, measurement uncertainty). This software delivers an optimized μCT resolution and enables data output in a common 3D format such as .raw used in this study. Smoothing and ring artifact correction were done automatically by the efX software for all volumes, and any additional manual filters were not applied. Beam hardening correction was set at 0.3 in the software

Data acquired from μCT was used to measure the volume percent mineral content in the demineralization windows of each sample. The μCT scan was transformed in 3-dimensions so that the surface of the sound window was perpendicular to the long-axis of the lesion. The same ROIs of 700-μm × 700-μm from the NIR SFE images were selected in the μCT scan images and the mean value of each layer was recorded to create a mineral density profile. The mineral density profile was converted to relative mineral density profile by assuming that sound enamel consisting of a maximum mineral density of 86 volume percent [34,35].

Lesion depths were estimated by comparing the relative mineral density profile of the lesion window to that of the sound window. From the edge of sound window, the volume percent mineral content over 200-μm depth was recorded. The relative integrated mineral loss (volume percent mineral loss × μm), ΔZ, was calculated by subtracting the volume percent mineral content of each lesion window from that of the sound window.

2.5 Statistical Analysis

Sample groups were compared using repeated measures one-way analysis of variance (ANOVA) with a Tukey–Kramer post hoc multiple comparison test. Linear regression analyses with robust standard least squares regression and robust generalized estimating equations (GEE) were used to examine the relationship between NIR SFE and μCT measurements. All statistical analyses were performed with 95% confidence with Prism™ (GraphPad software, San Diego, CA) and R 3.5.1 using the GEE package for generalized estimating equations.

3 Results

Figure 3 shows the visible reflectance image (a) and the μCT sectional image of a sample. Surface demineralization is clearly visible in the lesion windows. The sound window can be easily discerned from lesion windows by visual inspection. Lesion windows retained a red hue as it was difficult to completely remove protective red varnish even after immersion in acetone in an ultrasonic bath. This is most likely due to increased subsurface porosity from demineralization. The samples demonstrate a generalized increase in lesion depth and ΔZ with increased exposure to demineralization solution as shown in Table 1.

Figure 4 shows grayscale reflectance images taken of the dry and wet sample shown in Figure 3 using NIR SFE operating at 1310-nm and 1460-nm. Demineralized dry windows demonstrate a generalized increase in intensity compared to sound window and their wet counterparts. Images taken using 1310-nm light exhibit subsurface anatomical defects such as internal cracks. Images taken using 1460-nm light better visualize surface characteristics such as surface defects or porosity due to demineralization better than images taken using 1310-nm light. Even though the surfaces of the samples were tilted away from the perpendicular angle of the incident to eliminate specular reflection, trough lines between windows exhibited combination of specular reflection and strong scattering from roughened and angled trough surfaces. The specular reflection from the trough lines was much stronger in the wet sample due to water acting as smooth reflective surfaces.

Measurements from NIR SFE imaging of samples at both wet- and dry-conditions are shown in Table 2. The raw intensity measurements taken at dry-condition using 1460-nm light demonstrate significant differences between windows with an exception of the 32-hours window. The raw intensity measurements at dry-condition increased with an increase in lesion severity in

images taken both at 1310-nm and 1460-nm. There was a significant difference between the sound window and the demineralization window for the raw intensity measurements taken at dry-condition using 1460-nm light. However, the raw intensity measurements taken at dry-condition using 1310-nm light did not show a significant difference between the sound window and early demineralization windows, 8-hours and 16-hours. Raw intensity measurements taken at wet-condition were not significant at both 1310-nm and 1460-nm.

Other measurements were also taken at different conditions to determine the optimal method for differentiating lesion severity. Other measurement methods, such as intensity difference between dry and wet measurements and lesion contrast that have been previously employed in caries detection studies using NIR camera systems, were also compared [31,36]. Intensity difference values for both at 1310-nm and 1460-nm increased with an increase in exposure to the demineralization solution. Lesion contrast measured at 1460-nm was far greater than that measured at 1310-nm. It should be noted that there was high variance for intensity difference and lesion contrast measurements.

Once the raw intensity measurements at dry-condition using 1460-nm light were identified as the most optimal method for evaluating this NIR SFE prototype in this study, the measurements of the lesion windows were subtracted by the measurement of their corresponding sound windows for the linear regression analysis versus μCT measurements. The relative raw intensity measurements at dry-condition using 1460-nm light results are shown in Table 3.

Sensitivity analyses with robust standard least squares regression between the NIR SFE relative raw intensity measurements taken at dry-condition using 1460-nm light and μCT measurements were performed, and the results are shown in Table 4 and Figure 5. Sensitivity analysis involving robust GEE that accounted for correlation between windows from same

sample provided similar results as robust stand least squares regression. In general, the correlation analyses between the NIR SFE raw measurements at dry and lesion depth as well as ΔZ were moderately positive. It should be noted that p-values do not account for non-constant variance across different predictor values.

The diagnostic performance of the NIR SFE prototype at dry-condition using 1460-nm light was also evaluated. Each window of the sample was ranked in an increasing order in raw intensity measurements and the lowest ranking window was considered as a sound window. Sensitivity and specificity analysis is reported in Table 5. For all windows, sensitivity was 0.96 and specificity was 0.85. There were 3 false positives from sound windows and 3 false negatives originated from early demineralization windows; 2 false negatives were from 8-hours window and 1 false negative was from 16-hours window.

4 Discussion

This study evaluates the capability of the new NIR SFE device for detection of artificial caries lesions. Previous studies on InGaAs or Germanium CCD based camera systems operating at near-infrared wavelength have shown promise in detecting and assessing the severity of enamel caries lesions [37,38]. This study demonstrates that the NIR SFE is capable of detecting artificial caries lesions and differentiating between different lesions of varying severities. Raw intensity measurements taken at dry-condition using 1460-nm light (Table 2) showed the most significant differences between windows. Images taken at dry-condition (Figures 2a and 2c) showed an increase in raw intensity values because the air-filled pores on the surface mineral caused by demineralization act as a scattering medium. Images taken while wet (Figures 2b and 2d) showed dramatic reduction in raw intensity values as the pores are filled with water negating the strong scatter from the demineralized pores.

Other measurement techniques for analyzing NIR images from previous NIR camera studies were also explored in this study to evaluate the best technique for interpreting NIR SFE data [31,36]. The intensity difference measurements (Table 2) between dry and wet measurements and lesion contrast values showed an increasing trend with an increase in lesion depth and severity, these measurements did not yield as significant results as the raw intensity measurements taken from dry-condition suffered from high variance. Although the lesion contrast measurements (Table 2) at dry-condition were not significant between lesion windows at both 1310-nm and 1460-nm wavelengths, the reported contrast values at 1460-nm was more than 5 times higher than those at 1310-nm. Lesion contrast result shows that the images taken at 1460-nm provide superior contrast between sound and demineralized enamel than the images

taken at 1310-nm. This indicates that the 1460-nm is better suited for detection of demineralization than 1310-nm.

The NIR SFE prototype produced marked different images taken at 1310-nm and 1460-nm as shown in Figure 2. The images taken at 1460-nm showed much higher contrast images between sound and early demineralization (8- and 16-hours) than the images taken at 1310-nm. However, images taken at 1310-nm better depict internal flaws of the samples such as cracks that were most likely introduced during sample preparation because 1310-nm light penetrates enamel much further than 1460-nm light. The difference in the reflectance images captured at these two wavelengths is most likely due to increased water absorption at 1460-nm than 1310-nm [39].

There were moderate positive correlations between the NIR SFE relative raw intensity measurements taken at dry-condition using 1460-nm light and the μCT measurements; Pearson's r coefficients were 0.52 with the lesion depth and 0.51 with ΔZ (Table 4 and Figure 5). The NIR SFE prototype yielded strong diagnostic performance with high sensitivity (0.96) and specificity (0.85) as shown in Table 5. Variation in depths to underlying dentino-enamel junction and a potential specular reflection from underlying structure may have contributed to the increase in intensity of the false positive sound windows and the decrease in intensity of the false negative lesion windows. However, the three false negatives from early demineralization windows represent very shallow depth of remineralization (18.4-μm mean lesion depth for 8-hours window and 34.2-μm mean lesion depth for 16-hours window). Detection of early demineralization at such shallow depths is clinically insignificant. It is important to note that there was no false negative in the 24-hours and 32-hours windows, which represent lesions with greater depths (Table 1). These results demonstrate that the NIR SFE can be used as a predictor for detecting the presence of early demineralization and for assessing severity of the early lesion.

The samples prepared in this study had relatively shallow demineralization, up to 100-μm in depth, as verified by μCT measurements. With more severe lesions than the samples used in this study, future studies may be able to improve the correlation between the NIR SFE measurements and μCT measurements.

The samples used in this study are flat on the surface and the incident light from NIR SFE was intentionally angled to eliminate the specular reflection. The current shortcoming of this NIR SFE prototype is that the specular reflection cannot be eliminated from all angles of view. As the angulation between the surface of the sample and the incident light from NIR SFE vary depending on pixel location in the image, the reflectance raw values of one coordinate in the image to another coordinate are not uniform. There are multiple ways to address this issue. One possibility to overcome this problem is to use cross-polarizers between the laser source and the detector. Another possibility is to use multiple detectors and software optimization for elimination of specular reflection.

Another complication of NIR SFE system is that the measurement is dependent on the distance between the sample and the probe, since the detector in the NIR SFE system collects more photons when the sample is closer to the probe. In this study, all samples and windows were kept at approximately the same distance to reduce this effect, which would have influenced raw intensity values. The sample surface could have been slightly slanted due to errors introduced during sample preparation and mounting on the polyoxymethylene block. At 5mm probe-to-sample distance, even a small discrepancy in distance can influence the raw intensity measurements. To overcome this potential distance problem, lesion contrast measurement was also calculated, but the differences among windows were not significant from one another due to high variance. In a clinical setting, if the lesion is small, then imaging both the lesion and

surrounding sound enamel in the same field of view will allow an immediate lesion contrast measurement. However, using lesion contrast may present a challenge when the surface of the target is highly curved such as pits and fissure caries of the occlusal surfaces of the tooth. Multiple images can be taken at different angles to account for the irregular tooth surface morphology. Further study is required for testing NIR SFE for caries detection on non-smooth surfaces of the tooth.

5 Conclusions

In summary, the NIR SFE prototype can successfully differentiate between sound and demineralization on smooth enamel surface. The NIR SFE prototype at dry-condition using 1460-nm light was also capable of differentiating varying severity of demineralization. NIR wavelength 1460-nm was more suitable for quantifying superficial caries detection than 1310-nm. Although this study was conducted in a well-controlled manner, there are still necessary improvements to be made to reduce specular reflection and to optimize image quality and calibration. With the advantage of miniature probe size, maneuverability and real-time imaging speed, NIR SFE has strong potential to be employed in clinical settings for detecting and monitoring early caries lesions, such as WSLs.

6 Tables and Figures

Table 1. Mean ± S.D. for lesion depth and ΔZ from μCT measurements. Groups with the same letters are statistically similar, P > 0.05 in each row (n = 100).

	Sound	**8-hr Lesion**	**16-hr Lesion**	**24-hr Lesion**	**32-hr Lesion**
Lesion Depth (μm)	0 a	18.4±10.6 b	34.2±12.5 c	54.4±8.3 d	73.7±11.8 e
Relative Integrated Mineral Loss, ΔZ (vol% × μm)	0 a	809±589 b	1663±745 c	2687±644 d	3723±910 e

Table 2. Mean ± S.D. for raw intensity, intensity difference between dry and wet images, and lesion contrast values from NIR SFE measurements. Groups with the same letters are statistically similar, $P > 0.05$ in each row (n = 100).

	Sound	**8-hr Lesion**	**16-hr Lesion**	**24-hr Lesion**	**32-hr Lesion**
NIR SFE operating at 1310-nm					
Raw Intensity - Dry	92.7±31.3 a	108.3±31.5 a,b	116.9±28.7 a,b,c	126.2±31.7 b,c	130.4±34.3 c
Raw Intensity - Wet	91.6±31.2 a	96.7±27.5 a,b	98.1±23.3 a,b	99.4±33.1 a,b	109.4±38.0 b
Intensity Difference	1.1±7.0 a	11.7±13.9 b	18.7±22.6 a,b	26.8±21.0 c	21.0±22.1 b
Lesion Contrast[1] - Dry	-	0.11±0.27 a	0.17±0.30 a,b	0.25±0.21 a,b	0.28±0.17 b
NIR SFE operating at 1460-nm					
Raw Intensity - Dry	15.5±15.7 a	36.7±17.8 b	49.5±20.9 c	60.6±26.0 d	62.3±24.5 c,d
Raw Intensity - Wet	11.0±13.8 a	18.5±16.6 a	20.0±17.4 a	18.1±25.7 a	24.7±27.4 a
Intensity Difference	4.5±5.8 a	18.3±19.0 b	29.5±26.9 b,c	42.5±26.7 c	37.6±26.9 b,c
Lesion Contrast[1] - Dry	-	0.56±0.40 a	0.65±0.38 a,b	0.74±0.26 a,b	0.75±0.25 b

[1]Lesion contrast values were calculated based on individual raw intensity measurement.

[1]Number of windows analyzed for lesion contrast was 80 since sound windows were not included (n = 80).

Table 3. Mean ± S.D. for raw intensity measurements of lesion windows subtracted by the measurements of their corresponding sound windows from NIR SFE images at dry-condition using 1460-nm light. Groups with the same letters are statistically similar, $P > 0.05$ in each row ($n = 80$).

	8-hr Lesion	**16-hr Lesion**	**24-hr Lesion**	**32-hr Lesion**
Relative Raw Intensity (Lesion – Sound)	21.2±17.0 a	34.0±23.6 b	45.1±24.3 c	46.8±22.5 b,c

Table 4. p-value, Pearson's r and confidence interval for NIR SFE relative raw intensity measurements at dry-condition using 1460-nm light vs. μCT measurements (n = 80).

	p-value	**Pearson's r (lower CI[1], upper CI[1])**
Lesion Depth	< 0.0001	0.52 (0.34, 0.66)
Relative Integrated Mineral Loss, ΔZ	< 0.0001	0.51 (0.32, 0.65)

[1]CI: confidence interval

Table 5. Sensitivity and specificity analysis for NIR SFE measurements at dry-condition using 1460-nm light. A true positive represents a successful detection of demineralization and a true negative represents a successful detection of sound enamel.

	8-hr Lesion (n = 20)	**16-hr Lesion** (n = 20)	**24-hr Lesion** (n = 20)	**32-hr Lesion** (n = 20)	**All Windows** (n = 100)
Sensitivity	0.9	0.95	1	1	0.96
Specificity	-	-	-	-	0.85

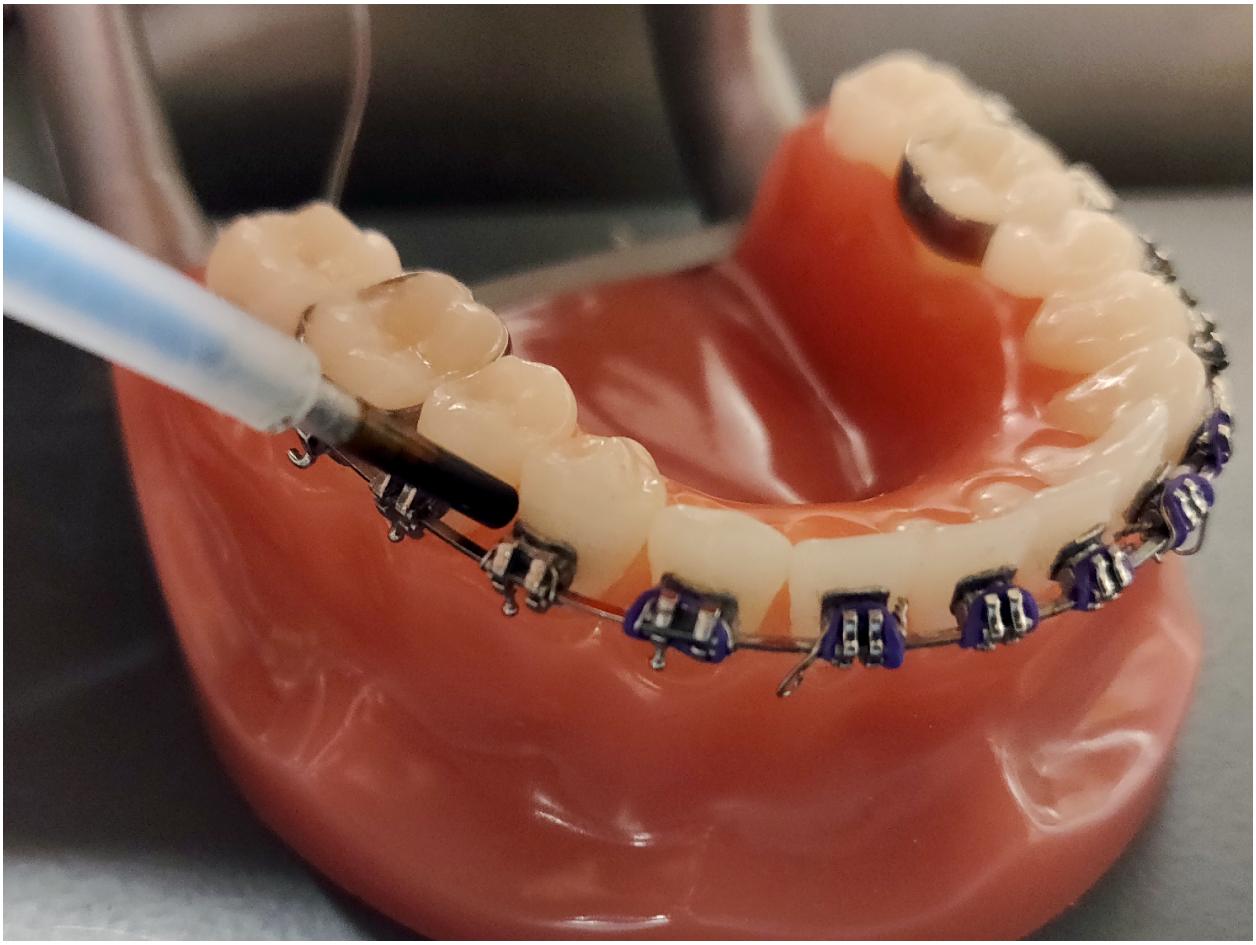

Figure 1. NIR SFE prototype on a typodont with orthodontic appliances.

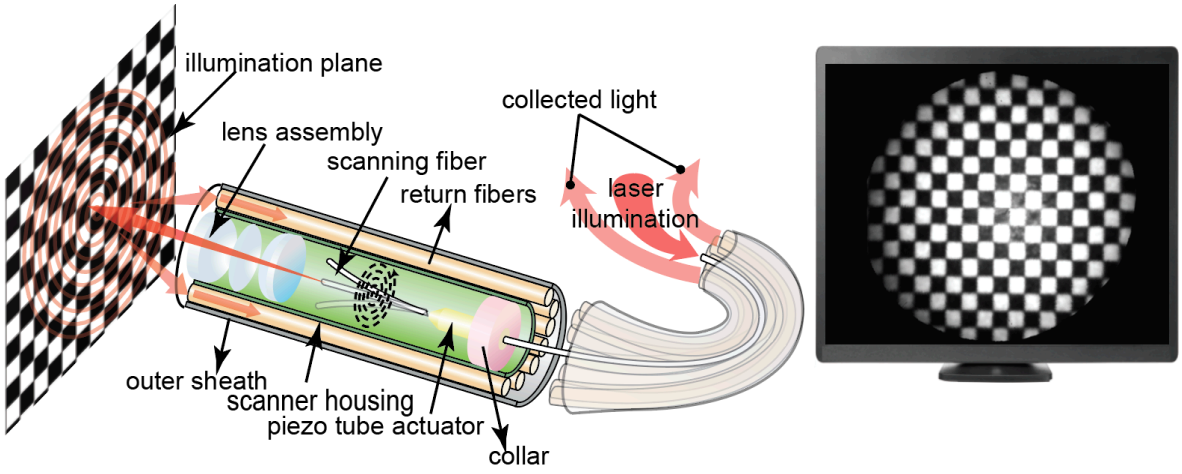

Figure 2. Schematic of NIR SFE probe imaging a checker board target. The image on the right shows the checker board target image captured by the NIR SFE operating at 1310-nm.

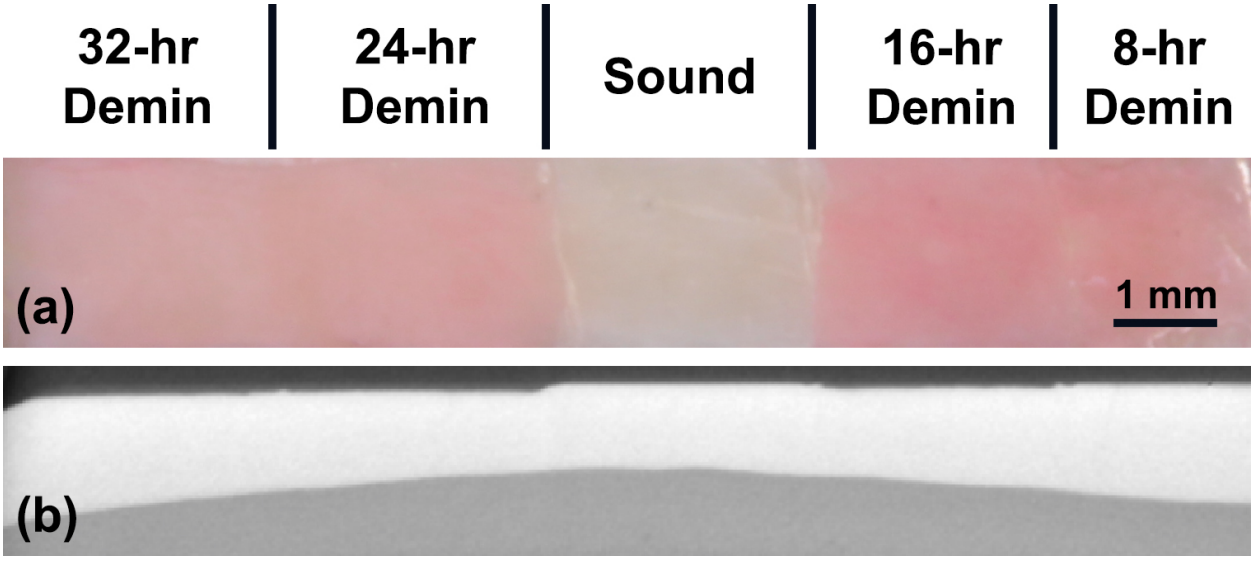

Figure 3. Visible light reflectance image (a) and the corresponding μCT section image (b).

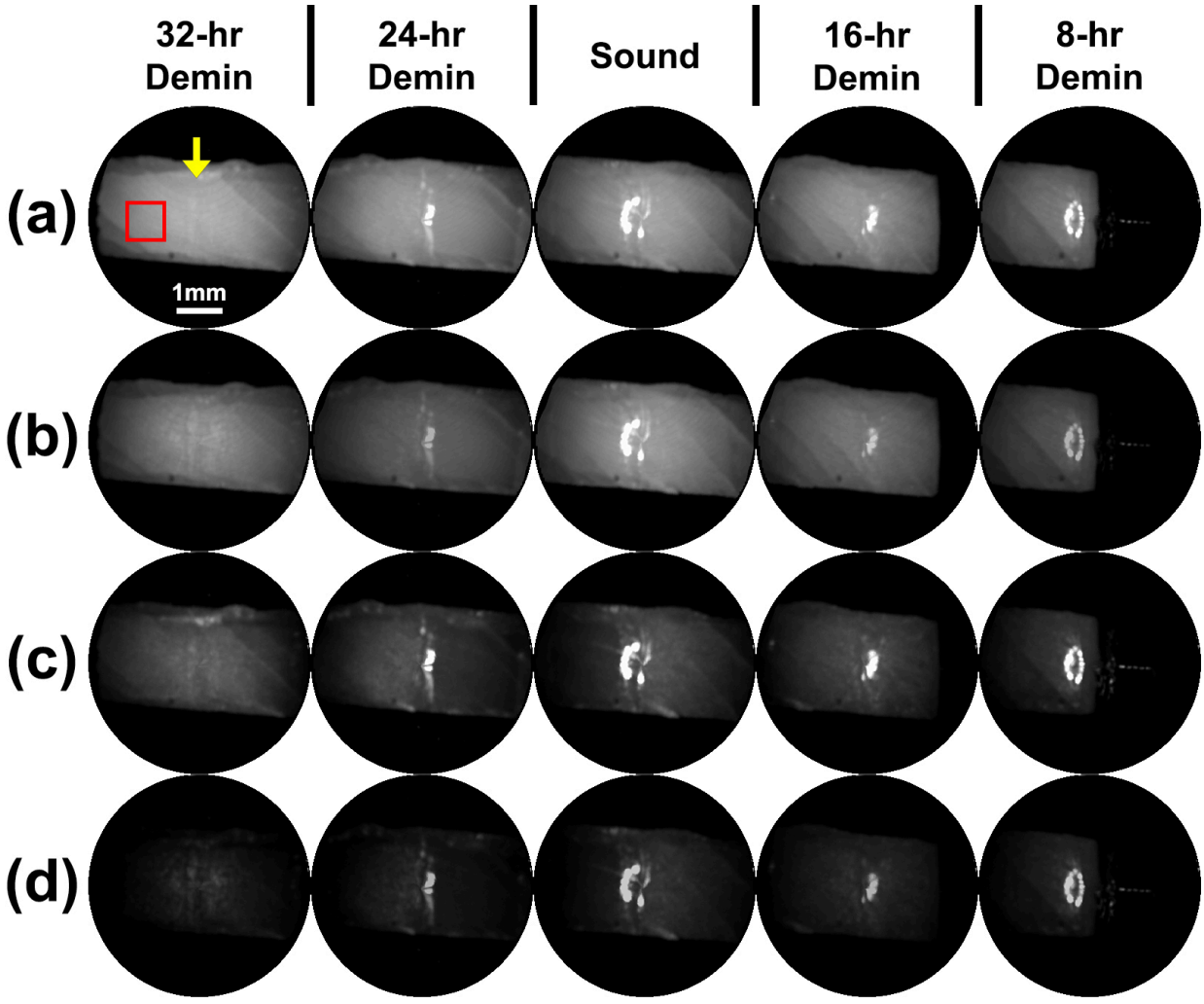

Figure 4. NIR SFE image of the sample shown in Figure 3. Four sets of images were taken: (a) dry sample imaged with SFE operating at 1310-nm, (b) wet sample imaged with SFE operating at 1310-nm, (c) dry sample imaged with SFE operating at 1460-nm, and (d) wet sample imaged with SFE operating at 1460-nm. Left window in the SFE field of view is the corresponding window labeled on the top. Red square box outlines the ROI where the mean value was recorded for statistical analysis. Same position of ROI was used for all images of each sample. Yellow arrow indicates the trough line dividing two windows shown in an image frame.

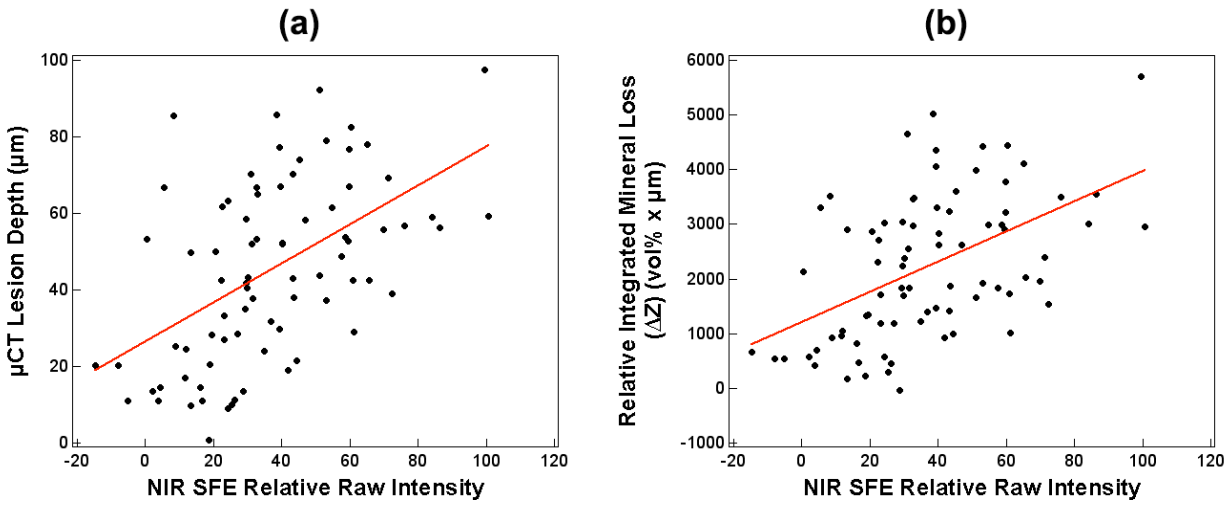

Figure 5. Plots of NIR SFE relative raw intensity measurements at dry-condition using 1460-nm light vs. (a) lesion depth and (b) relative integrated mineral loss (n = 80).

7 References

1. NIDCR. Oral health in America: a report of the surgeon general - executive summary; U.S. Department of Health and Human Services, National Institute of Dental and Craniofacial Research, National Institutes of Health: Rockville, MD, 2000.

2. Dye, B.A.; Tan, S.; Smith, V.; Lewis, B.G.; Barker, L.K.; Thornton-Evans, G.; Eke, P.I.; Beltran-Aguilar, E.D.; Horowitz, A.M.; Li, C.H. Trends in oral health status: United States, 1988-1994 and 1999-2004. *Vital Health Stat.* **2007**, *11*, 1-92.

3. Marinho, V.C.; Worthington, H.V.; Walsh, T.; Chong, L.Y. Fluoride gels for preventing dental caries in children and adolescents. *The Cochrane Database Syst. Rev.* **2015**, *6*, 1-114.

4. Marinho, V.C.; Worthington, H.V.; Walsh, T.; Clarkson, J.E. Fluoride varnishes for preventing dental caries in children and adolescents. *The Cochrane Database Syst. Rev.* **2013**, *7*, 1-95.

5. Kaste, L.M.; Selwitz, R.H.; Oldakowski, R.J.; Brunelle, J.A.; Winn, D.M.; Brown, L.J. Coronal caries in the primary and permanent dentition of children and adolescents 1-17 years of age: United States, 1988-1991. *J. Dent. Res.* **1996**, *75*, 631-641.

6. Chauncey, H.H.; Glass, R.L.; Alman, J.E. Dental caries, principal cause of tooth extraction in a sample of US male adults. *Caries Res.* **1989**, *23*, 200-205.

7. Carvalho, J.C. Caries process on occlusal surfaces: evolving evidence and understanding. *Caries Res.* **2014**, *48*, 339-346.

8. Sawle, R.F.; Andlaw, R.J. Has occlusal caries become more difficult to diagnose? A study comparing clinically undetected lesions in molar teeth of 14-16-year old children in 1974 and 1982. *Br. Dent. J.* **1988**, *164*, 209-211.

9. Hannigan, A.; O'Mullane, D.M.; Barry, D.; Schafer, F.; Roberts, A.J. A caries susceptibility classification of tooth surfaces by survival time. *Caries Res.* **2000**, *34*, 103-108.

10. Tellez, M.; Gomez, J.; Kaur, S.; Pretty, I.A.; Ellwood, R.; Ismail, A.I. Non-surgical management methods of noncavitated carious lesions. *Community Dent. Oral Epidemiol.* **2013**, *41*, 79-96.

11. Featherstone, J.D.B. Prevention and reversal of dental caries: role of low level fluoride. *Community Dent. Oral Epidemiol.* **1999**, *27*, 31-40.

12. Chang, H.S.; Walsh, L.J.; Freer, T.J. Enamel demineralization during orthodontic treatment. Aetiology and prevention. *Aust. Dent. J.* **1997**, *42*, 322-327.

13. Lopatiene, K.; Borisovaite, M.; Lapenaite, E. Prevention and treatment of white spot lesions during and after treatment with fixed orthodontic appliances: a systematic literature review. *J. Oral Maxillofac. Res.* **2016**, *7*, 1-11.

14. National Institutes of Health Consensus Development Panel. Diagnosis and management of dental caries throughout life. National Institute of Health Consensus Development Conference statement, March 26-28, 2001. *J. Dent. Educ.* **2001**, *65*, 1162-1168.

15. Ekstrand, K.R.; Zero, D.T.; Martignon, S.; Pitts, N.B. Lesion activity assessment. *Monogr. Oral. Sci.* **2009**, *21*, 63-90.

16. Bader, J.D.; Shugars, D.A.; Bonito, A.J. A systematic review of the performance of methods for identifying carious lesions. *J. Public Health Dent.* **2002**, *62*, 201-213.

17. Braga, M.M.; Mendes, F.M.; Ekstrand, K.R. Detection activity assessment and diagnosis of dental caries lesions. *Dent. Clin. North Am.* **2010**, *54*, 479-493.

18. Featherstone, J.D.B. Clinical Implications: New strategies for caries prevention. Proceedings of Annual Indiana Conference: Early Detection of Dental Caries, Indianapolis, IN, USA, 1996; Stookey, G.K. Ed.; pp. 287-296.

19. Staninec, M.; Douglas, S.M.; Darling, C.L.; Chan, K.; Kang, H.; Lee, R.C.; Fried, D. Nondestructive clinical assessment of occlusal caries lesions using near-IR imaging methods. *Lasers in Surg. Med.* **2011**, *43*, 951-959.

20. Hafström-Björkman, U.; Sundström, F.; Jong, E.d.J.d.; Oliveby, A.; Angmar-Månsson, B. Comparison of laser fluorescence and longitudinal microradiography for quantitative assessment of in vitro enamel caries. *Caries Res.* **1992**, *26*, 241-247.

21. Kaneko, K.; Matsuyama, K.; Nakashima, S. Quantification of early carious enamel lesions by using an infrared camera. Proceedings of Annual Indiana Conference: Early detection of Dental caries II, Indianapolis, IN, USA, 1999; Stookey, G.K. Ed.; pp. 83-99.

22. Fried, D.; Glena, R.E.; Featherstone, J.D.; Seka, W. Nature of light scattering in dental enamel and dentin at visible and near-infrared wavelengths. *Appl. Opt.* **1995**, *34*, 1278-1285.

23. Jones, R.S.; Fried, D. Attenuation of 1310- and 1550-nm laser light through sound dental enamel. Proceedings of International Symposium on Biomedical Optics: Lasers in Dentistry VIII, 2002; 4610, pp. 187-190.

24. Buhler, C.; Ngaotheppitak, P.; Fried, D. Imaging of occlusal dental caries (decay) with near-IR light at 1310-nm. *Opt. Express* **2005**, *13*, 573-582.

25. Fried, W.A.; Fried, D.; Chan, K.H.; Darling, C.L. High contrast reflectance imaging of simulated lesions on tooth occlusal surfaces at near-IR wavelengths. *Lasers Surg. Med.* **2013**, *45*, 533-541.

26. Simon, J.C.; Chan, K.H.; Darling, C.L.; Fried, D. Multispectral near-IR reflectance imaging of simulated early occlusal lesions: variation of lesion contrast with lesion depth and severity. *Lasers Surg. Med.* **2014**, *46*, 203-215.

27. Zhang, L.; Nelson, L.Y.; Seibel, E.J. Spectrally enhanced imaging of occlusal surfaces and artificial shallow enamel erosions with a scanning fiber endoscope. *J. Biomed. Opt.* **2012**, *17*, 076019.

28. Zhang, L.; Kim, A.S.; Ridge, J.S.; Nelson, L.Y.; Berg, J.H.; Seibel, E.J. Trimodal detection of early childhood caries using laser light scanning and fluorescence spectroscopy: clinical prototype. *J. Biomed. Opt.* **2013**, *18*, 111412.

29. Staninec, M.; Lee, C.; Darling, C.L.; Fried, D. In vivo near-IR imaging of approximal dental decay at 1,310 nm. *Lasers Surg. Med.* **2010**, *42*, 292-298.

30. Zhou, Y.; Lee, R.C.; Finkleman, S.; Sadr, A.; Seibel, E. J. Near-infrared multispectral endoscopic imaging of deep artificial interproximal lesions in extracted teeth. *Lasers Surg. Med.* **2019**, In Press.

31. Lee, R.C.; Darling, C.L.; Fried, D. Assessment of remineralization via measurement of dehydration rates with thermal and near-IR reflectance imaging. *J. Dent.* **2015**, *43*, 1032-1042.

32. Lee, C.; Lee, D.; Darling, C.L.; Fried, D. Nondestructive assessment of the severity of occlusal caries lesions with near-infrared imaging at 1310 nm. *J. Biomed. Opt.* **2010**, *15*, 047011..

33. Hamba, H.; Nikaido, T.; Sadr, A.; Nakashima, S.; Tagami, J. Enamel lesion parameter correlations between polychromatic micro-CT and TMR. *J. Dent. Res.* **2012**, *91*, 586-591.

34. Angmar, B.; Carlstrom, D.; Glas, J.E. Studies on the ultrastructure of dental enamel. IV. The mineralization of normal human enamel. *J. Ultrastruct. Res.* **1963**, *8*, 12-23.

35. de Josselin de Jong, E.; ten Bosch, J.J.; Noordmans, J. Optimised microcomputer-guided quantitative microradiography on dental mineralised tissue slices. *Phys. Med. Biol.* **1987**, *32*, 887-899.

36. Wu, J.; Fried, D. High contrast near-infrared polarized reflectance images of demineralization on tooth buccal and occlusal surfaces at lambda = 1310-nm. *Lasers Surg. Med.* **2009**, *41*, 208-213.

37. Zakian, C.; Pretty, I.; Ellwood, R. Near-infrared hyperspectral imaging of teeth for dental caries detection. *J. Biomed. Opt.* **2009**, *14*, 064047.

38. Lee, C.; Darling, C.L.; Fried, D. In vitro near-infrared imaging of occlusal dental caries using a germanium enhanced CMOS camera. Proceedings of International Symposium on Biomedical Optics: Lasers in Dentistry XVI, 2010; 75490K, pp. 1-7.

39. Hale, G.M.; Querry, M.R. Optical constants of water in the 200-nm to 200-µm wavelength region. *Appl. Optics.* **1973**, *12*, 555-563